JOURNAL OF GUIDANCE, CONTROL, AND DYNAMICS
Vol. 15, No. 3, May-June 1992

Robust Wind Shear Stochastic Controller-Estimator

R. K. Prasanth,* J. E. Bailey,† and K. Krishnakumar‡
University of Alabama, Tuscaloosa, Alabama 35487

This study analyzes airplane wind shear flight-path control and state estimation in the presence of uncertainties in microburst size and strength. Variations in wind shear shaping filter parameters are computed using a theoretical wind model that agrees in spectral characteristics with actual microbursts. Stratonovich interpretation of stochastic integrals is used to derive a coupled linear quadratic controller-estimator system. Verification of design robustness is carried out using both nonlinear and linearized Boeing 727 longitudinal approach and takeoff flight simulations. Linear simulation results for the coupled system are compared with those for a linear quadratic Gaussian reference design to show improvement in performance. Monte Carlo simulation with nonlinear apprach and takeoff models demonstrates robustness of the coupled controller-estimator system with respect to variations in microburst size and strength.

I. Introduction

CONTROL of airplane flight through a microburst has received considerable attention in the recent past. Miele et al.,[1-3] Psiaki and Stengal,[4,5] and Bryson and Zhao[6] have investigated optimal control laws and feedback strategies for flight in the presence of wind shear. Flight simulation and airplane performance studies have shown that optimal management of airplane energy is fundamental in controlling flight through a microburst. Jones[7] and Lambregts[8] introduced energy management concepts and energy-based guidance systems for broad applications encompassing microburst encounter. Krishnakumar and Bailey[9] studied performance of an inertial energy distribution (IED) controller in a microburst environment. Bossi and Bryson[10] pioneered research in the dual aspect of wind shear state estimation using Kalman filtering techniques. Onboard implementation of control strategies require estimation of aircraft and wind states.

Guidance law validation procedures employed in previous research assume exact knowledge of aircraft and wind shear states. Although used as a means to circumvent estimation of wind shear states, this assumption results in overly optimistic performance from the guidance system. Moreover, recent developments in control theory[11] have shown that the separation principle upon which the assumption is based is not valid when parameter uncertainties are present. Significant variations in microburst size (1-4 km) and differential velocity (10-50 m/s) of a statistical nature occur in reality. In such instances, linear quadratic Gaussian (LQG) controller-estimator design, which requires exact a priori knowledge of system parameters, postulates the use of a nominal system model (e.g., an average microburst), and variations from the nominal microburst are assumed negligible. Performance of the system so synthesized degrades when a priori conditions change. In a microburst encounter, the aircraft is forced into a maximum performance situation with limited energy resources and control system sensitivity to a priori conditions can degrade controller performance.

A fresh treatment of the microburst controller-estimator problem, which results in the design of a coupled system that is robust with respect to variations in microburst size and strength, is presented herein. The controller objectives of interest in this study relate to the use of a wind shear tailored autopilot that is active for all landings and takeoffs of an aircraft. This concept is in contrast to wind shear detection followed by a guidance law implementation. Interest in this problem originates from the fact that aircraft have inadvertent encounters with large microbursts as well as many encounters with small, nonkiller microbursts in their normal environment. The design synthesis utilizes a theoretical microburst model that agrees in spectral characteristics with actual microbursts. Monte Carlo simulation using nonlinear approach and takeoff models with feedback provided by the linear coupled controller estimator is used to verify robust performance. Results from linear flight simulation are compared with those from a baseline LQG design to show improvement in controller and estimator performances.

II. Controller-Estimator Design

Let the system and measurement models be described by the autonomous equations:

$$dx = [A_n\,dt + A_i\,d\alpha]x + [B_n dt + B_i\,d\alpha]u(t) + C\,d\eta \qquad (1)$$

$$x(0) = x_0, \qquad t \geq 0$$

$$y(t) = [H_n + H_i\gamma]x(t) + N\nu(t)$$

where A_n, A_i, B_n, C, H_n, and H_i are matrix-valued bounded measurable functions; $\alpha(t)$ and $\eta(t)$ are unit-diffusion vector Brownian motion processes; and $\nu(t)$ and $\gamma(t)$ are convenient notations for unit-diffusion vector Brownian motion processes

$$\int_0^t \nu(\tau)\,d\tau, \qquad \int_0^t \gamma(\tau)\,d\tau$$

Further, let u belong to a set of nonanticipatory (admissible) measurable Markov control functions Ω. We are interested in finding a control function $u^*(t) \in \Omega$ that is progressively measurable with respect to the natural filtration of $x(.)$, measurable with respect to the σ algebra generated by parameter uncertainties, and achieves the infimum of the quadratic cost functional

$$J(x,u,t) = E\left[\int_0^T (x^T,\, u^T)\begin{pmatrix} W_{11} & 0 \\ 0 & W_{22} \end{pmatrix}\begin{Bmatrix} x \\ u \end{Bmatrix} dt\right]$$

where W_{11} and W_{22} are symmetric nonnegative and positive definite functions, respectively.

Unlike LQG design ($A_i = B_i = H_i = 0$), Itô and Stratonovich interpretations of the stochastic differential equation (1) yield as solutions homogeneous Markov processes that differ

Received February 1, 1990; revision received July 1, 1991; accepted for publication July 10, 1991.

*Graduate Student, Department of Aerospace Engineering, Box 870280.
†Professor, Department of Aerospace Engineering, Box 870280.
‡Assistant Professor, Department of Aerospace Engineering, Box 870280.

in drift behavior. Therefore, prior to applying Bellman's optimality principle, the interpretation that correctly describes the physical process must be agreed upon. In the Itô theory, there is a certain kind of separation between the effects of diffusion and drift. However, the physical process modeled by Eq. (1), past diffusion affects future drift because uncertainties in system parameters that cause drift are modeled using a pure diffusion process. The Stratonovich interpretation takes into account this effect and has the physical appeal of being the limit of a sequence of ordinary differential equations. Further, the time-asymmetric nature of Itô integral leads to the uncertainty threshold principle,[12] which precludes the existence of stable solutions beyond a quantifiable threshold of uncertainty. For these reasons, Eq. (1) will be interpreted as a Stratonovich equation. The unique advantages lost in interpreting Eq. (1) in a Stratonovich sense can be regained by shifting back to a corrected Itô equation using the Stratonovich averaging procedure.[13] The corrected Itô equation is given by

$$dx(t) = [A_c\,dt + A_i\,d\alpha]x(t) + [B_c\,dt + B_i\,d\alpha]u(t) + C\,d\eta(t)$$

$$x(0) = x_0, \qquad t \geq 0$$

$$y(t) = [H_c + H_i\gamma]x(t) + N\nu(t)$$

$$A_c = A_n + \tfrac{1}{2}A_i^2, \qquad B_c = B_n + \tfrac{1}{2}A_iB_i, \qquad H_c = H_n + \tfrac{1}{2}H_iA_i$$

For the Stratonovich corrected Itô stochastic equation, there exists a unique homogeneous Markov process as its solution. Application of Bellman's optimality principle then gives

$$\inf_u [A^u J(t, \hat{x}) + L] = 0$$

where A^u is the infinitesimal generator for the Itô stochastic equation. Following Borkar[14] and Bryson and Ho,[15] the stochastic minimization problem can be transformed into a deterministic problem. The conditions given in the following are obtained by applying variational principles:

$$A_cP + PA_c^T + C_i\hat{P}C_i^T - GP_c^T + Q + A_iPA_i^T = 0$$

$$SA_c + A_c^TS + E_i^T\hat{S}E_i + W_{11} - S_c^TK + A_i^TSA_i = 0$$

$$(A_c - B_cK)\hat{P} + \hat{P}(A_c - B_cK)^T + GP_c^T = 0$$

$$(A_c - GH_c)^T\hat{S} + \hat{S}(A_c - GH_c) + S_c^TK = 0$$

$$F = A_c - GH_c - B_cK, \qquad C_i = A_i - B_iK$$

$$E_i = A_i - GH_i, \quad G = P_cR_c^{-1}, \quad K = W_{2c}^{-1}S_c$$

$$P_c = PH_c^T + A_i(P + \hat{P})H_i^T, \qquad S_c = B_c^TS + B_i^T(S + \hat{S})A_i$$

$$R_c = R_1 + H_i(P + \hat{P})H_i^T, \qquad W_{2c} = W_{22} + B_i^T(S + \hat{S})B_i$$

These equations form a coupled system of algebraic Riccati and Lyapunov (Sylvestor) equations that must be solved simultaneously for steady-state controller and estimator gains. An iterative technique using Schur decomposition can be used for solution.[16] For brevity, the controller estimator given by this coupled system will be referred to as the coupled linear quadratic system (CLQS).

Microburst size and strength can only be described statistically, that is, as a random variable with a well-defined probability distribution function. Because of this lack of a priori knowledge, microburst wind shaping filter parameters that depend on the size and strength become random variables themselves. The use of multiplicative white processes is important in modeling these variations. The matrices A_n and A_i can be thought of as the average and the variance of the system parameters that are uncertain. An unbiased unique construction of these matrices is a well-known inverse problem whose solution is given by the maximum entropy principle.[17]

III. Microburst Wind Model

Statistical data on microburst phenomena that are currently available are not sufficient to allow a direct evaluation of probability distribution functions for shaping filter parameters. Therefore, a theoretical model consistent with the observed statistical nature of microbursts is needed to estimate these distributions. A microburst model used extensively is the Zhu-Etkin fluid dynamic model,[18] wherein the microburst outflow is modeled as an irrotational flow emanating from a spatial vortex distribution. By adjusting the size of the vortex and/or its strength distribution, microbursts of varying sizes and differential velocities can be generated. Theoretical simplicity and minimal computing requirements make the Zhu-Etkin model an attractive choice for real-time flight simulation.

Figure 1 compares the power spectra of the microburst winds that caused the Dallas-Fort Worth (DFW) Delta 191 air accident with those of the corresponding Zhu-Etkin wind time histories. The apparent discrepancy in spectral density at higher frequencies can be attributed to the presence of high-frequency turbulence in the DFW microburst. Figure 2 shows the effect of adding Dryden spectra turbulence to the Zhu-Etkin microburst. The excellent agreement in low- and high-frequency spectra forms the basis for modeling microburst wind as the sum of Zhu-Etkin wind shear and Dryden spectra turbulence. Implicit in the model is the assumption that turbulence and microburst wind shear can be modeled independently. Technically, inferences can be made only from an expected spectral density computed as an ensemble average. The primary use of the DFW power spectrum is not in statistical inference but in showing that the Zhu-Etkin microburst power spectral density can be scaled to match those for measured microburst spectra and can serve as the basis for microburst shaping filter design.

Nonstationary effects are induced by spatial and temporal microburst characteristics. However, in this analysis, stationary processes are used to approximate microburst wind. Experimental evidence suggests that turbulence length scales increase through a microburst[19] and in some hitherto unknown manner depend on microburst size and strength. Such a functional dependence between turbulence and microburst

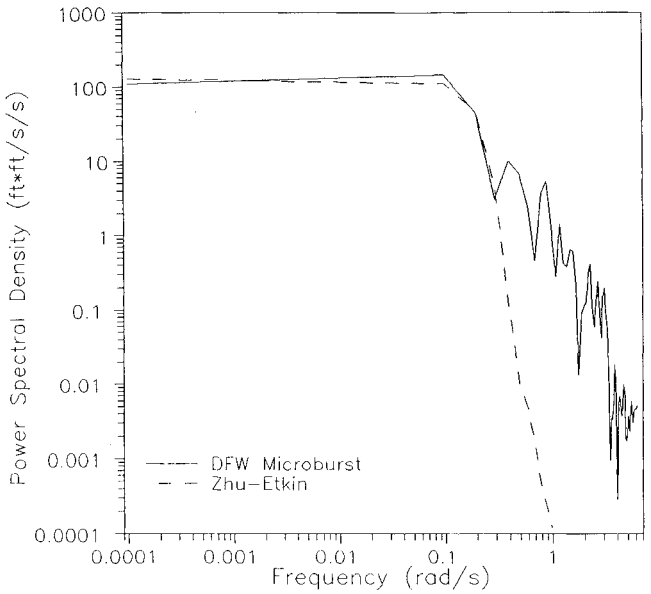

Fig. 1 Comparison of DFW microburst power spectra with scaled Zhu-Etkin microburst.

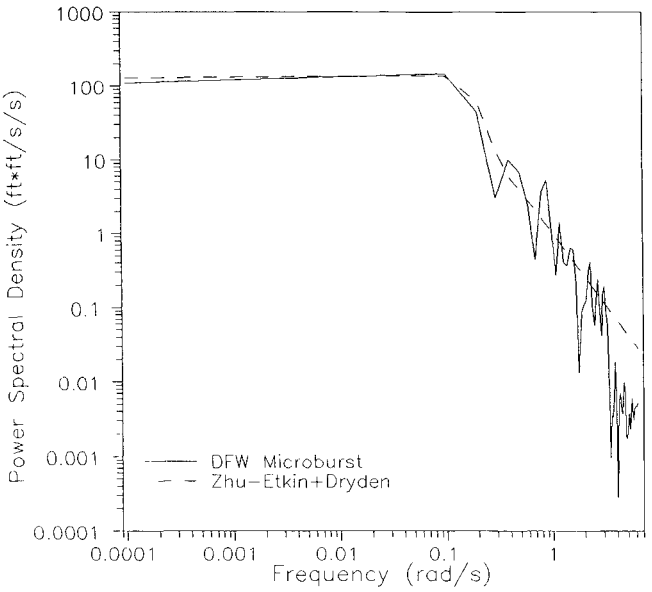

Fig. 2 Comparison of DFW microburst power spectra with scaled Zhu-Etkin and Dryden turbulence.

parameters will result in a nonstationary and non-Gaussian wind process description. This functional dependence is neglected in this analysis to provide a simplified microburst wind shaping filter design.

The procedure for wind shear shaping filter design begins by assuming a uniform distribution for Zhu-Etkin microburst vortex size and Gaussian distribution for vortex strength. This statistical description of Zhu-Etkin microburst wind velocity is consistent with the Joint Airport Weather Studies (JAWS) data.[20] Next, the joint probability distribution function for microburst wind velocity along a straight-line path is estimated from an ensemble of randomly drawn Zhu-Etkin microbursts. The shaping filter process model is then assumed to be given by

$$dW = [A_n\, dt + A_i\, d\alpha]W + C\, d\eta$$

where $W = [a_x, w_x, a_z, w_z]$ is the wind shear state vector. The unknown shaping filter parameters that generate the joint distribution function can be computed by minimizing the square error between the shaping filter process moments and the corresponding moments of the distribution. Parameter optimization techniques such as the genetic algorithm can be used for this purpose.[21]

It needs to be emphasized that the use of the Zhu-Etkin model was prompted by limited statistical data on microbursts. When sufficient experimental data become available, theoretical models can be relinquished for a more direct evaluation of shaping filter parameters.

IV. Verification of Design Robustness

The previous sections presented a microburst controller-estimator design methodology that takes into account variations in microburst size and strength. In this section, we describe Monte Carlo simulation studies conducted to evaluate performance and robustness characteristics of the CLQS. First, we use a linear approach model (see Appendix) and flight simulation to compare performance of CLQS with a reference LQG design. Next, robustness of the CLQS with respect to variations in microburst size and strength is demonstrated with nonlinear approach and takeoff flight simulations. External disturbances used in Monte Carlo simulations consist of Zhu-Etkin microburst and Dryden spectra turbulence. The CLQS state-space model and measurements are

$$dx(t) = (A_n\, dt + A_i\, d\alpha)x(t) + (B_n\, dt + B_i\, d\alpha)u(t) + d\eta(t)$$

$$y(t) = (H_n + H_i\alpha)x(t) + \nu(t)$$

where

$$x^T = [w \quad x_I \quad z_I \quad u \quad w \quad \theta \quad q \quad \delta_t]$$

$$w = [a_x \quad w_x \quad a_z \quad w_z \quad t_x \quad t_z], \quad u^T = [\delta_{th} \quad \delta_e]$$

$$\eta^T = [\eta_1 \quad \eta_2 \quad \eta_3 \quad \eta_4 \quad \eta_5 \quad \eta_6]$$

$$E[\eta(t)] = 0, \qquad E[\eta(t)\eta^T(t)] = Q$$

$$y^T = [x_I \quad z_I \quad u \quad w \quad \theta \quad q \quad \delta_t]$$

$$E[\nu(t)] = 0, \qquad E[\nu(t)\nu^T(\tau)] = R\delta(t-\tau)$$

In these equations, α_x, w_x, a_z, w_z, and t_x, t_z are wind shear and turbulence states, respectively; whereas u, w, q, and θ are aircraft states and x_I, z_I are kinematic states. The delayed response of aircraft engines to throttle control is approximated by a first-order transfer function (δ_t/δ_{th}). The quadratic

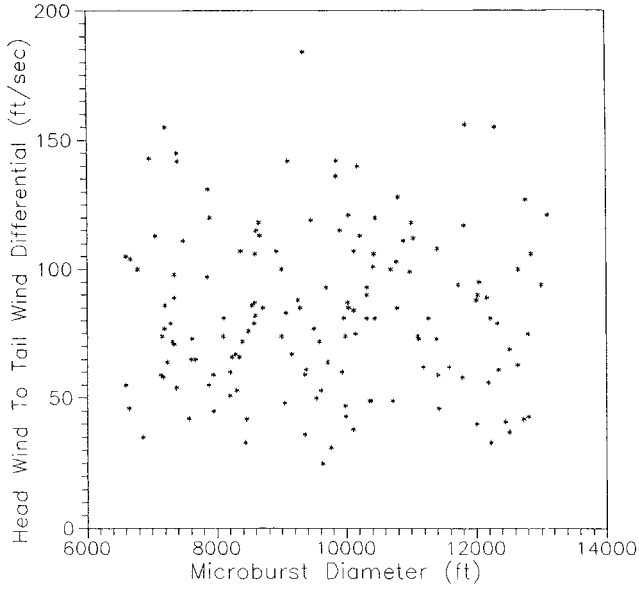

Fig. 3 Zhu-Etkin microburst sample for Monte Carlo simulation (linear and nonlinear models).

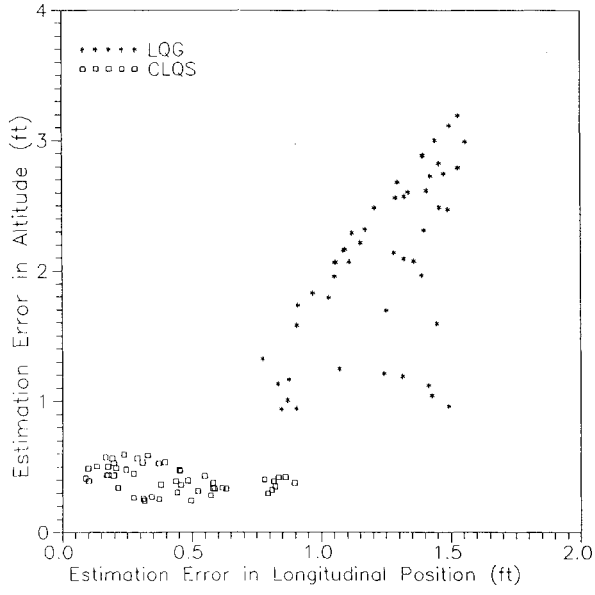

Fig. 4 LQG and CLQS performance comparison Monte Carlo simulation—linear approach model.

cost functional that approximates the IED controller is given by[9]

$$J(x, u) = E\left[\frac{1}{2}\int_{t_0}^{t_f}\left\{x^T W_{11} x + u^T W_{22} u\right\} \mathrm{d}t\right]$$

where

$$W_{11} = A_n^T C C^T A_n, \qquad W_{22} = B_n^T C C^T B_n$$

The reference LQG controller estimator (uncoupled) used for performance comparison uses the Bossi-Bryson wind shear estimator[10] and the inertial distribution controller. The following subsections summarize linear and nonlinear simulations.

Linear Simulation

The purpose here is to compare the performance of the CLQS with that of the LQG design. Flight through a large number of randomly drawn Zhu-Etkin microbursts and Dryden spectra turbulence is simulated using a linearized Boeing 727 longitudinal approach model. The performances of

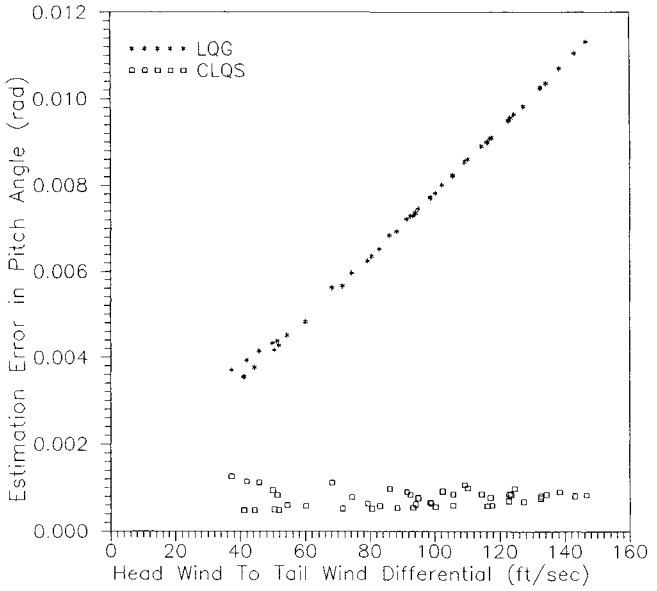

Fig. 5 LQG and CLQS performance comparison Monte Carlo simulation—linear approach model.

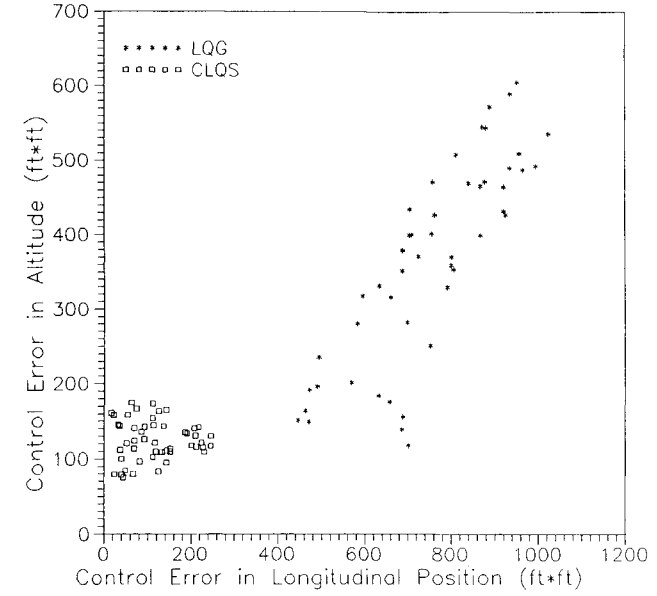

Fig. 6 LQG and CLQS performance comparison Monte Carlo simulation—linear approach model.

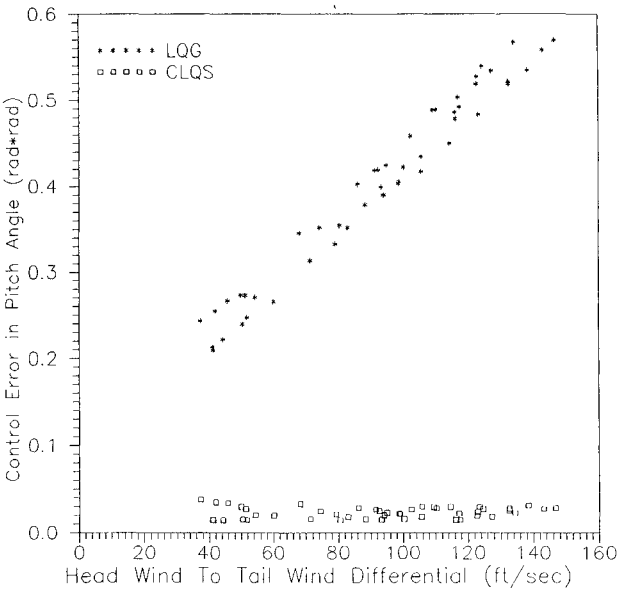

Fig. 7 LQG and CLQS performance comparison Monte Carlo simulation—linear approach model.

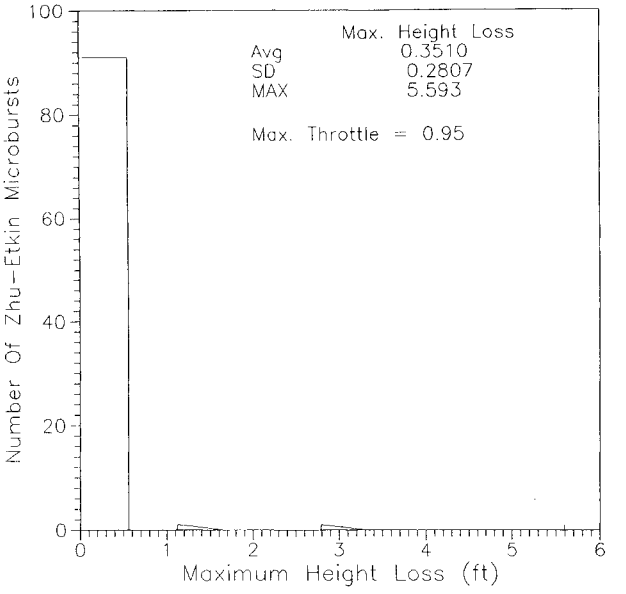

Fig. 8 CLQS performance—Monte Carlo simulation with nonlinear approach model.

the estimator and the controller are computed for each microburst using the following definitions:

$$X_e = \frac{1}{T}\int_0^T |x_{\text{actual}} - x_{\text{est}}| \, \mathrm{d}t$$

$$X_c = \frac{1}{T}\int_0^T x_{\text{actual}}^2 \, \mathrm{d}t$$

where X_e is a scalar-valued average estimation error in state $x(t)$ and X_c is scalar-valued mean square deviation from glide slope in $x(t)$.

Zhu-Etkin microbursts used for the Monte Carlo simulation are shown in Fig. 3. Figures 4–7 compare the performance of the CLQS with that for the baseline LQG design. A general appreciation of the figures indicates that controller and estimator errors are significantly reduced by incorporating statistical information on microburst parameters in the system model. Further, the CLQS sensitivity to variations in microburst size and strength is minimal.

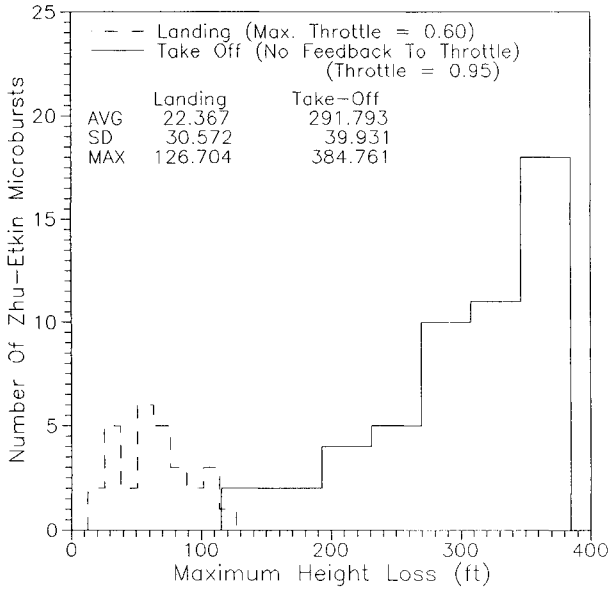

Fig. 9 CLQS performance—Monte Carlo simulation with nonlinear approach and takeoff.

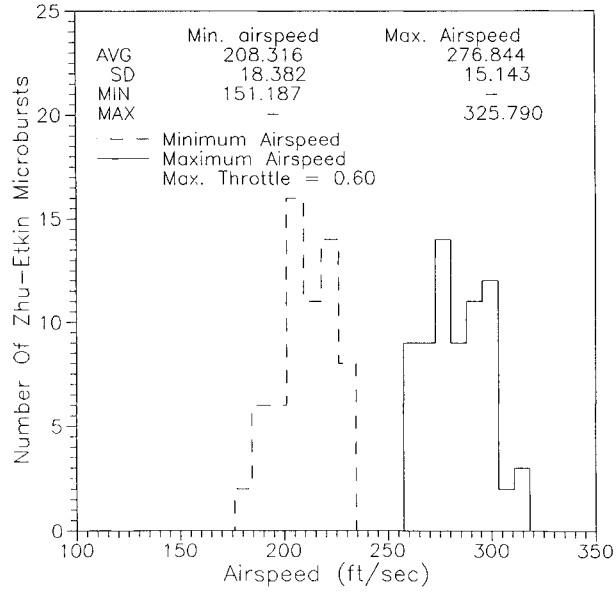

Fig. 10 CLQS performance—Monte Carlo landing simulation using nonlinear model.

Table 1 Statistics of nonlinear approach ($\delta_{max} = 0.6$) flight simulation using the coupled linear quadratic system

	Height loss	Minimum airspeed	Maximum airspeed	Minimum inertial speed	Maximum inertial speed
Average	22.366	208.316	276.844	233.716	243.610
SD	30.571	18.381	15.143	7.704	8.685
Minimum	—	151.187	—	221.895	—
Maximum	126.704	—	325.79	—	259.841

Table 2 Statistics of nonlinear takeoff flight simulation using the coupled linear quadratic system

	Height loss	Minimum airspeed	Maximum airspeed	Minimum inertial speed	Maximum inertial speed
Average	291.793	230.395	301.877	268.114	275.579
SD	39.931	19.613	16.813	4.240	4.340
Minimum	—	176.854	—	260.849	—
Maximum	384.761	—	341.234	—	284.348

Nonlinear Simulation

Monte Carlo simulation using a nonlinear flight dynamics model is used to demonstrate robustness of the CLQS with respect to variations in microburst size and strength. The nonlinear body axis equations of motion used for takeoff and approach simulations are the following:

$$\dot{X}_I = U\cos\theta + W\sin\theta$$

$$\dot{H}_I = U\sin\theta + W\cos\theta$$

$$m\dot{U} = L\sin\alpha - D\cos\alpha - mg\sin\theta - mWq + (T\cos\delta)\delta_t$$

$$m\dot{W} = D\sin\alpha - L\cos\alpha + mg\sin\theta - mUq - (T\sin\delta)\delta_t + Z_e\delta_e$$

$$\dot{q} = M_u u + M_w w + M_q q + M_t\delta_t + M_e\delta_e + (M_u\cos\theta_0 + M_w\sin\theta_0)W_x - (M_u\sin\theta_0 - M_w\cos\theta_0)W_z$$

$$\dot{\theta} = q, \qquad \dot{\delta}_t = \frac{\delta_t - \delta_{th}}{\tau}$$

$$0.05 = \delta_{t\,\min} \le \delta_t \le \delta_{t\,\max} = 0.95$$

$$-0.4363 = \delta_{e\,\min} \le \delta_e \le {}_{e\,\max} = 0.3054$$

$$\alpha_B \le \alpha_{\max} = 0.2443$$

$$T = T(V_A,\beta), \quad L = L(V_A,\alpha), \quad D = D(V_A,\alpha)$$

$$W_X = W_X(X_I,H_I), \qquad W_Z = W_Z(X_I,H_I)$$

$$W_x = W_X\cos\gamma_A - W_Z\sin\gamma_A$$

$$W_z = W_X\sin\gamma_A - W_Z\cos\gamma_A$$

$$\alpha = \tan^{-1}\frac{W - W_z}{U - W_x}, \qquad \gamma_A = \tan^{-1}\frac{\dot{H}_I - W_Z}{\dot{X}_I - W_X}$$

where W_X and W_Z are external disturbances composed of randomly drawn Zhu-Etkin microburst and Dryden spectra turbulence. Control feedback and state estimation are provided by the coupled controller-estimator system designed using the linearized (trim level flight) Boeing 727 model. A detailed description of the model including trim parameters is given in Ref. 21.

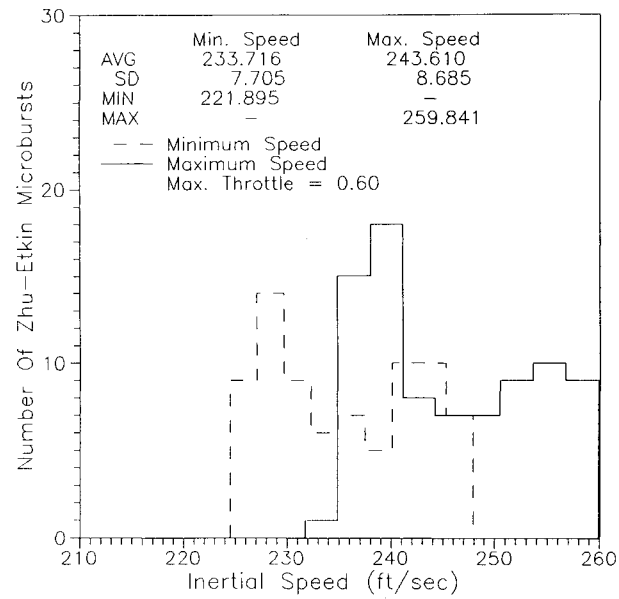

Fig. 11 CLQS performance—Monte Carlo landing simulation using nonlinear model.

Table 3 Comparison of nonlinear takeoff simulation statistics using the coupled linear quadratic system with results from Ref. 21

		Height loss	Minimum airspeed	Maximum airspeed	Minimum inertial speed	Maximum inertial speed
Average	Ref. 21	319.42	234.9	312.3	258.15	277.8
Average	Present	291.793	230.395	301.877	268.114	275.579
SD	Ref. 21	155.3	15.25	12.79	8.73	1.85
SD	Present	39.931	19.613	16.813	4.240	4.340

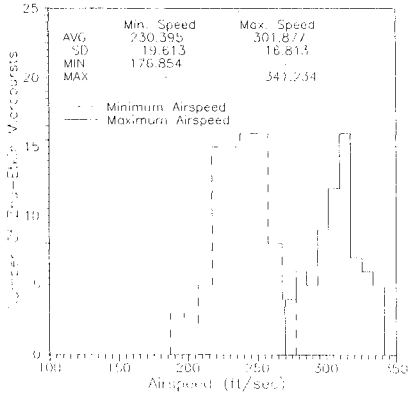

Fig. 12 CLQS performance—Monte Carlo takeoff simulation using nonlinear model.

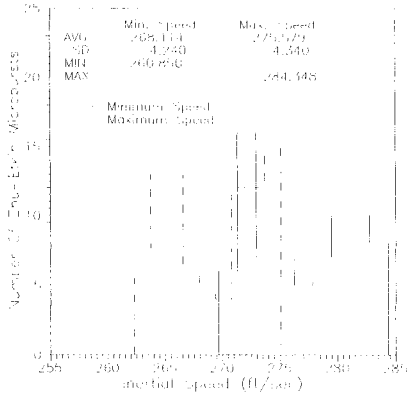

Fig. 13 CLQS performance—Monte Carlo takeoff simulation using nonlinear model.

In an effort to study the effects of maximum throttle control limits, approach simulation is carried out for two values of δ_{max}. With δ_{max} at 0.95 (that is, 65% in excess of $\delta_{trim} = 0.30$), sufficient energy was available for the aircraft to fly through all microbursts without any significant height loss (Fig. 8). Maximum height loss increased to about 130 ft with $\delta_{max} = 0.6$ (Fig. 9). This indicates that allowing large excursions in throttle can significantly reduce height loss in approach. Takeoff simulations are carried out with constant throttle setting ($\delta_t = 0.95$). Histograms of Figs. 8–13 show the number of microbursts (out of 200) that had specified ranges of variation in height loss, airspeed, and inertial speed. it must be observed that trim airspeed for approach and takeoff are, respectively, 237 and 277 ft/s. Tables 1 and 2 summarize the results of the Monte Carlo simulation for approach and takeoff airspeed, inertial speed and height loss.

References 9 and 21 compare the performance of the inertial distribution controller with those for MIN MAX γ and MIN MAX height loss controllers assuming perfect knowledge of wind states and no turbulence. Comparison of the present results (Table 3) with those of Ref. 9 and 21 show significantly lower variations in maximum height loss which demonstrate robustness with respect to changes in microburst size and strength. Average height loss and airspeed variations of the present study also compare reasonably well with those given in Refs. 9 and 21.

V. Conclusions

State dependent noise processes are used to include microburst size and strength variations in the system model. A coupled controller-estimator system is derived and implemented using Stratonovich interpretation of stochastic integrals. The design equations were numerically solved for linearized Boeing 727 longitudinal approach and takeoff models. System robustness with respect to variations in microburst size and strength is demonstrated using nonlinear flight simulation. Comparison of performance with an LQG reference design shows significant improvement. The following can be concluded:

1) Stratonovich interpretation of stochastic systems can be used to include parameter uncertainty in controller-estimator design.

2) The resulting coupled controller-estimator system performs significantly better than an LQG design.

3) Nonlinear Monte Carlo flight simulations demonstrate robustness of the CLQS with respect to variations in microburst size and strength.

Appendix: Controller-Estimator Database for Landing

$$A = [A_1 \quad A_2], \qquad A_i = [A_3 \quad A_4]$$

$$E[\beta\beta^T] = [Q_1 \quad Q_2], \qquad E[\nu(t)\nu(\tau)^T] = R\,\delta(t-\tau)$$

$$A_1 = \begin{bmatrix} -0.0063 & -0.0565 & 0 & 0 & 0 & 0 \\ 0.0691 & -0.0063 & 0 & 0 & 0 & 0 \\ 0 & 0 & -0.0063 & -0.0725 & 0 & 0 \\ 0 & 0 & -0.0823 & -0.0063 & 0 & 0 \\ 0 & 0 & 0 & 0 & -0.1633 & 0 \\ 0 & 0 & 0 & 0 & 0 & -0.2371 \\ 0 & 0 & 0 & 0 & 0 & 0 \\ 0 & 0 & 0 & 0 & 0 & 0 \\ 0 & 0.0170 & 0 & 0.1180 & 0.0170 & 0.1180 \\ 0 & 0.2450 & 0 & -0.4390 & 0.2450 & -0.4390 \\ 0 & 0 & 0 & 0 & 0 & 0 \\ 0 & 0 & 0 & -0.0050 & 0 & -0.0050 \\ 0 & 0 & 0 & 0 & 0 & 0 \end{bmatrix}$$

$$R = \begin{bmatrix} 4 & 0 & 0 & 0 & 0 & 0 \\ 0 & 5 & 0 & 0 & 0 & 0 \\ 0 & 0 & 2 & 0 & 0 & 0 \\ 0 & 0 & 0 & 3 & 0 & 0 \\ 0 & 0 & 0 & 0 & 0.003 & 0 \\ 0 & 0 & 0 & 0 & 0 & 0.003 \\ 0 & 0 & 0 & 0 & 0 & 0.003 \end{bmatrix}$$

$$A_2 = \begin{bmatrix} 0 & 0 & 0 & 0 & 0 & 0 & 0 \\ 0 & 0 & 0 & 0 & 0 & 0 & 0 \\ 0 & 0 & 0 & 0 & 0 & 0 & 0 \\ 0 & 0 & 0 & 0 & 0 & 0 & 0 \\ 0 & 0 & 0 & 0 & 0 & 0 & 0 \\ 0 & 0 & 0 & 0 & 0 & 0 & 0 \\ -0.005 & 0 & 0.999 & 0.041 & 12.298 & 0 & 0 \\ 0 & -0.005 & 0.041 & -0.999 & 236.801 & 0 & 0 \\ 0 & 0 & -0.022 & 0.114 & -32.172 & -22.149 & 8.514 \\ 0 & 0 & -0.234 & -0.447 & -1.339 & 232.307 & -0.297 \\ 0 & 0 & 0 & 0 & 0 & 1.000 & 0 \\ 0 & 0 & 0 & -0.005 & 0 & -0.330 & 0 \\ 0 & 0 & 0 & 0 & 0 & 0 & -0.500 \end{bmatrix}$$

$$W_{22} = \begin{bmatrix} 3000 & 0 \\ 0 & 2357.37 \end{bmatrix}$$

$$B_n^T = \begin{bmatrix} 0 & 0 & 0 & 0 & 0 & 0 & 0 & 0 & 0 & 0 & 0 & 0 & 0.5 \\ 0 & 0 & 0 & 0 & 0 & 0 & 0 & 0 & 0 & -2.192 & 0 & -0.519 & 0 \end{bmatrix}$$

$$B_i = 0, \qquad H_i = 0, \qquad Q_2 = 0$$

$$H_n^T = \begin{bmatrix} 0 & 0 & 0 & 0 & 0 & 0 & 1 & 0 & 0 & 0 & 0 & 0 & 0 \\ 0 & 0 & 0 & 0 & 0 & 0 & 0 & 1 & 0 & 0 & 0 & 0 & 0 \\ 0 & 0 & 0 & 0 & 0 & 0 & 0 & 0 & 1 & 0 & 0 & 0 & 0 \\ 0 & 0 & 0 & 0 & 0 & 0 & 0 & 0 & 0 & 1 & 0 & 0 & 0 \\ 0 & 0 & 0 & 0 & 0 & 0 & 0 & 0 & 0 & 0 & 1 & 0 & 0 \\ 0 & 0 & 0 & 0 & 0 & 0 & 0 & 0 & 0 & 0 & 0 & 1 & 0 \\ 0 & 0 & 0 & 0 & 0 & 0 & 0 & 0 & 0 & 0 & 0 & 0 & 1 \end{bmatrix}$$

$$Q_1 = \begin{bmatrix} 9 & 0 & 0 & 0 & 0 & 0 & 0 & 0 & 0 & 0 & 0 & 0 & 0 \\ 9 & 0 & 0 & 0 & 0 & 0 & 0 & 0 & 0 & 0 & 0 & 0 & 0 \\ 9 & 0 & 0 & 0 & 0 & 0 & 0 & 0 & 0 & 0 & 0 & 0 & 0 \\ 9 & 0 & 0 & 0 & 0 & 0 & 0 & 0 & 0 & 0 & 0 & 0 & 0 \\ 9 & 0 & 0 & 0 & 0 & 0 & 0 & 0 & 0 & 0 & 0 & 0 & 0 \\ 9 & 0 & 0 & 0 & 0 & 0 & 0 & 0 & 0 & 0 & 0 & 0 & 0 \end{bmatrix}$$

$$A_3 = \begin{bmatrix} -0.1000 & 1.1000 & 0 & 0 & 0 & 0 \\ -0.9000 & -0.1000 & 0 & 0 & 0 & 0 \\ 0 & 0 & -0.1000 & 1.1000 & 0 & 0 \\ 0 & 0 & -0.9000 & -0.1000 & 0 & 0 \\ 0 & 0 & 0 & 0 & 0 & 0 \\ 0 & 0 & 0 & 0 & 0 & 0 \\ 0 & 0 & 0 & 0 & 0 & 0 \\ 0 & 0 & 0 & 0 & 0 & 0 \\ 0 & 0 & 0 & 0 & 0 & 0 \\ 0 & 0 & 0 & 0 & 0 & 0 \\ 0 & 0 & 0 & 0 & 0 & 0 \\ 0 & 0 & 0 & 0 & 0 & 0 \\ 0 & 0 & 0 & 0 & 0 & 0 \end{bmatrix}$$

$$A_4 = \begin{bmatrix} 0 & 0 & 0 & 0 & 0 & 0 & 0 \\ 0 & 0 & 0 & 0 & 0 & 0 & 0 \\ 0 & 0 & 0 & 0 & 0 & 0 & 0 \\ 0 & 0 & 0 & 0 & 0 & 0 & 0 \\ 0 & 0 & 0 & 0 & 0 & 0 & 0 \\ 0 & 0 & 0 & 0 & 0 & 0 & 0 \\ -0.5 & 0 & 0 & 0 & 0 & 0 & 0 \\ 0 & -0.5 & 0 & 0 & 0 & 0 & 0 \\ 0 & 0 & 0 & 0 & 0 & 0 & 0 \\ 0 & 0 & 0 & 0 & 0 & 0 & 0 \\ 0 & 0 & 0 & 0 & 0 & 0 & 0 \\ 0 & 0 & 0 & -0.5 & 0 & 0 & 0 \\ 0 & 0 & 0 & 0 & 0 & 0 & 0 \end{bmatrix}$$

$$W_{11} = \begin{bmatrix} 0 & 0 & 0 & 0 & 0 & 0 & 0 & 0 & 0 & 0 & 0 & 0 & 0 \\ 0 & 89.1 & 0 & 171 & 89.1 & 171 & 0 & 1.5 & -110 & 464 & -143,959 & -786 & 18,912 \\ 0 & 0 & 0 & 0 & 0 & 0 & 0 & 0 & 0 & 0 & 0 & 0 & 0 \\ 0 & 171 & 0 & 328 & 171 & 328 & 0 & 2.9 & -212 & 891 & -276,533 & -1511 & 36,328 \\ 0 & 89.1 & 0 & 171 & 89.1 & 171 & 0 & 1.5 & -110 & 464 & -143,959 & -786 & 18,912 \\ 0 & 171 & 0 & 328 & 171 & 328 & 0 & 2.9 & -212 & 891 & -276,533 & -1511 & 36,328 \\ 0 & 0 & 0 & 0 & 0 & 0 & 0 & 0 & 0 & 0 & 0 & 0 & 0 \\ 0 & 1.5 & 0 & 2.9 & 1.5 & 2.9 & 0 & 0.026 & -1.8 & 7.9 & -2455 & -13.4 & 322 \\ 0 & -110 & 0 & -212 & -110 & -212 & 0 & -1.8 & 136 & -575 & 178,378 & 974 & -23,433 \\ 0 & 464 & 0 & 891 & 464 & 891 & 0 & 7.9 & -575 & 2418 & -749,984 & -4098 & 98,527 \\ 0 & -143,959 & 0 & -276,533 & -143,959 & -276,533 & 0 & -2455 & 178,378 & -7.9e05 & 2.3e07 & 1.2e06 & -3.0e07 \\ 0 & -786 & 0 & -1511 & -786 & -1511 & 0 & 13.4 & 974 & -4098 & 1.2e06 & 6944 & 166,955 \\ 0 & 18,912 & 0 & 36,328 & 18,912 & 36,328 & 0 & 322 & -23,433 & 98,527 & -3.0e07 & -1.6e05 & 4.0e06 \end{bmatrix}$$

References

[1]Miele, A., Wang, T., and Melvin, W. W., "Optimal Flight Trajectories in the Presence of Wind Shear, Part 1, Equations of Motion," Rice Univ., Houston, TX, Aero-Astronautics Rept. 191, 1985.

[2]Miele, A., Wang, T., and Melvin, W. W., "Optimal Flight Trajectories in the Presence of Wind Shear, Part 2, Problem Formulation," Rice Univ., Houston, TX, Aero-Astronautics Rept. 192, 1985.

[3]Miele, A., Wang, T., and Melvin, W. W., "Optimal Flight Trajectories in the Presence of Wind Shear, Part 4, Numerical Results," Rice Univ., Houston, TX, Aero-Astronautics Rept. 194, 1985.

[4]Psiaki, M. L., and Stengel, R. F., "Optimal Flight Paths Through Microburst Wind Profiles," *Journal of Aircraft,* Vol. 23, No. 8, 1986, pp. 629–635.

[5]Psiaki, M. L., and Stengel, R. F., "Analysis of Aircraft Control Strategies for Microburst Encounter," *Journal of Guidance, Control, and Dynamics,* Vol. 8, No. 5, 1985, pp. 553–559.

[6]Bryson, A. E., and Zhao, Y., "Feedback Control for Penetrating a Microburst," AIAA Paper 87-2343, AIAA Guidance, Navigation, and Control Conference, Aug. 1987.

[7]Jones, J. G., "Application of Energy Management Concepts to Path Control in Turbulence," AGARD-CP-140, 1973.

[8]Lambregts, A. A., "Vertical Flight Path and Speed Control Autopilot Design Using Total Energy Principles," AIAA Paper 83-2239, 1983.

[9]Krishnakumar, K., and Bailey, J. E., "Inertial Energy Distribution Error Control for Optimal Wind Shear Penetration," *Journal of Guidance, Control, and Dynamics,* Vol. 13, No. 6, 1990, pp. 994–951.

[10]Bossi, J. A., and Bryson, A. E., "Disturbance Estimation for a STOL Transport During Landing," *Journal of Guidance, Control, and Dynamics,* Vol. 5, No. 3, May 1982, pp. 258–262.

[11]Hyland, D. C., "Maximum Entropy Stochastic Approach to Controller Design for Uncertain Structural Systems," American Control Conference, June 1982.

[12]Athans, M., Ku, R., and Gershwin, S. B., "The Uncertainty Threshold Principle: Some Fundamental Limitations of Optimal Decision Making Under Dynamic Uncertainty," *IEEE Transactions on Automatic Control,* June 1977.

[13]Wong, E., and Zakai, M., "On the Relation Between Ordinary and Stochastic Differential Equations," *International Journal of Engineering Sciences,* Vol. 3, 1965.

[14]Borkar, V. S., *Optimal Control of Diffusion Processes*, Pitman Research Notes in Mathematics, Longman, London, 1989.

[15]Bryson, A. E., and Ho, Y., *Applied Optimal Control,* Wiley, New York, 1975.

[16]Prasanth, R. K., "A New Approach to Wind Shear Controller and Estimator Design," M.S. Thesis, Univ. of Alabama, Tuscaloosa, AL, Dec. 1989.

[17]Jaynes, E. T., "Where Do We Go From Here?" *Maximum Entropy and Bayesian Methods in Inverse Problems,* edited by C. R. Smith and W. T. Grandy, Jr., D. Reidel Publishing, Boston, MA, 1985.

[18]Zhu, S., and Etkin, B., "Model of the Wind Field in a Downburst," *Journal of Aircraft,* Vol. 22, No. 7, 1985, pp. 595–601.

[19]Campbell, C. W., "A Spatial Model of Wind Shear and Turbulence for Flight Simulation," NASA TP-2313, 1984.

[20]McCarthy, J., "Recommendations for Coping with Microburst Wind Shear: An Aviation Hazard," *Journal of Air Law and Commerce,* Vol. 49, No. 2, 1984.

[21]Krishnakumar, K. S., "Energy Concepts Applied to Control of Airplane Flight in Wind Shear," Ph.D. Dissertation, Univ. of Alabama, Tuscaloosa, AL, May 1988.